KSCE Journal of Civil Engineering (2022) 26(8):3342-3354
DOI 10.1007/s12205-022-5369-3

pISSN 1226-7988, eISSN 1976-3808
www.springer.com/12205

Geotechnical Engineering

Shaking Table Test Study on Dynamic Response of Bedding Rock Slope with Weak Rock

Mingzhu Guo[a], **Chen Wang**[a], **He Zhang**[b], **Kunsheng Gu**[a], **and Huang Liu**[a]

[a]*Dept. of Urban Construction, Beijing University of Technology, Beijing 100124, China*
[b]*Hebei Provincial Seismological Bureau, Shijiazhuang 050021, China*

ARTICLE HISTORY

Received 6 August 2021
Revised 1st 19 October 2021
Revised 2nd 1 December 2021
Accepted 14 February 2022
Published Online 27 June 2022

KEYWORDS

Shaking table test
Bedding rock slope
Acceleration dynamic response
Failure mechanism
Weak rock layer

ABSTRACT

A shaking table model test was conducted to study the dynamic response and failure mechanism of a bedding rock slope with weak rock layer based on the "Xiaguiwa" landslide in the Jinsha River basin of Sichuan-Tibet. The influence of schist-like weak rock layer on bedding rock slope is considered. The test results show that the Peak Ground Acceleration (PGA) amplification coefficient varies rhythmically from the inside to the surface of the slope, and 0.3 g and 0.6 g are the slope appears cracking and instability. schist-like weak rock layer makes the seismic wave enhance obviously, but in the slope flexure position, the seismic wave near the weak rock layer is slightly weakened instead, and the maximum displacement often occurs above the weak rock layer. the "bucking" occurs at 1/4 of the slope height, and the fracture degree at the middle and lower part of the slope is greater than that at the middle and upper part, and the slope damage surface appears to be "concave at the top and convex at the bottom". The damage process of the model slope is divided into four stages. The model test results reflect the influence of the weak rock layer on the seismic dynamic response and damage process of the bedding rock slope.

1. Introduction

Layered rock slopes are common in engineering. Under the action of external forces such as earthquakes, precipitation, and manual excavation, large-scale landslides can develop, endangering lives and property (Liu, 2014). Layered rock slopes are usually classified according to the structural relationship between the rock layer and the slope surface. They can be categorized as nearly horizontal, bedding, oblique, and counter-bedding slopes (Wang and Cun, 2008). A bedding slope is a layered slope whose slope direction and inclination are similar to the rock layer. The bedding and lithological interfaces are the dominant surfaces for slope sliding; The slope with an obvious layered structure has poor stability. The failure of bedding rock slope with weak structure due to sudden sliding, fast speed and large volume is noteworthy and disastrous (Hoek and Bray, 1981). Typical examples include the Donghekou landslide, the Daguangbao landslide, the Ganmofang landslide in Qingchuan County and Tsaoling landslide (Chigira et al., 2003; Huang et al., 2008; Xu and Dong, 2011; Deng et al., 2016). Many researchers have begun to study the role of structural planes, weak rock layers, and other dominant surfaces in bedding rock landslides, and analyze the dynamic response laws of such slopes to ensure the slope stability subject to earthquakes and precipitation (Fan, 2016; Li et al., 2019).

Studying the dynamic response and failure mechanism of bedding rock slopes includes three main methods: field surveys (Aydan, 2016; Li et al., 2021), numerical simulations (Abe et al., 2017; Lv et al., 2017), and model tests (Clough and Pirtz, 1956; Wartman et al., 2005). The earthquake simulation shaking table test is a type of model test. Strong operability and repeatability can intuitively and efficiently reflect the prototype's response law and failure mechanism under different external force environments (Zhang et al., 2019). Researchers have designed shaking table tests for different types of bedding rock slopes, revealing the influence of the structure on the dynamic response of layered rock slopes. Men et al. (2004) designed bedding rock slopes with faults, using shaking table test to analyze the influence of seismic amplitude, slope structure, and other factors on slope failure. Xu et al. (2010) and Liu et al. (2012) used slope tests in hardness-upward and softness-upward lithology to demonstrate the

CORRESPONDENCE He Zhang hebgcy@163.com Hebei Provincial Seismological Bureau, Shijiazhuang 050021, China

impacts of lithological interfaces on slopes, and the amplitude amplification effect of seismic waves in different frequency bands. Fan et al. (2016a) used model tests of bedding and counter-bedding slopes containing thin weak rock layers to verify the "height effect" and "surface-tending effect" of the PGA amplification coefficient, showing the upper and lower sides of the thin interlayer and the volatility growth of the PGA amplification coefficient. Xu et al. (2008) designed a bedding slope test with soil layers to explain the soil's high-frequency filtering and low-frequency amplification of the seismic wave, verifying that the significant period of the input earthquake is close to the natural vibration period of the slope. During the vibration period, the PGA amplification coefficient increases. The model tests of Zhou et al. (2016) and Zhou et al. (2020) showed that the impact of weak interlayers on seismic waves is different in different directions. Modal analysis verifies that the weak interlayer has a different impact on the slope. The control effect of deformation occurs mainly in the third-order mode. Chen et al. (2020) analyzed the propagation and energy density distribution of seismic waves and found that the potential damage area and damage location of the slope is closely related to the energy density distribution. Song et al. (2019) researched that the inherent high-frequency component of the wave causes local deformation of the slope, the low-frequency component causes overall instability. The high-frequency component controls the progressive failure of the slope. Fan et al. (2016b) used the shaking table test marginal spectrum to characterize the model slope's internal seismic damage development process. Slope instability is controlled mainly by the weak rock layer. Deng et al. (2020) used shaking table test to study the dynamic stability of bedding rock slopes with different slope heights, slope angles, layer inclination and layer thickness under frequent microearthquakes. Huang et al. (2013), Jia (2011) and Yang et al. (2012) revealed the response characteristics and lithology of multi-lithological bedding rock slopes through shaking table tests with the PGA amplification coefficient and the critical displacement as indicators.

Shaking table tests have become a common method for studying the dynamic response of bedding rock slopes under seismic loads; however, most tests have shortcomings in selecting input seismic waves and the construction of model slopes. Previous studies rarely consider the location of the study area when selecting seismic waves and mainly focused on simple horizontal structural surfaces and weak linear interlayers. In this study, a shaking table test was conducted to investigate the seismic dynamic response law and the deformation and failure process of a typical bedding rock slope in the Jinsha River basin. It is more consistent with the site characteristics of the Jinsha River basin to select Maoxian and Wolong measured seismic waves. For the model slopes, four sizes of adobe test blocks were produced to simulate geological conditions with complicated development of rock layered joints on the rock slope, and reproduce the "burst" phenomenon on the rock slope along the bedding. The test plan is optimized from the seismic input and model structure. The acceleration response law of the bedding slope is studied, and the influence of the weak rock layer on the dynamic response law in the slope is analyzed. The results reasonably explain the starting mechanism and failure mode of the "Xiaguiwa" landslide, and provide a reference for the Jinsha River basin landslide control and engineering disaster reduction.

2. Test Overview

2.1 Overview of Landslide Prototype

The "Xiaguiwa" landslide is located in Suwalong Township, in the upper reaches of the Jinsha River at the junction of Sichuan and Tibet (Fig. 1). It is a typical bedding collapse and damage landslide, historically causing blockage of the Jinsha River. The landslide area is located 1.8 km west of the Suwalong-Wangdalong fault zone and 1 km east of the western branch of the nearly north-south regional Jinsha River main fault. It is a regional fault confluence zone. The lithology of the exposed strata includes Lower Permian P1 amphibolite Ψo, partially intercalated with marble and granite veins, and Quaternary Holocene Q4 alluvial, alluvial proluvial, and colluvial deposits. Amphibolite is the main lithology of the "Xiaguiwa" landslide; the mica schist is a weak rock layer with an average thickness of 3 m. The outcropping rock layer is located at SW257° ∠35°; the slope is developed with complete gullies, and the overall connectivity of the terrain is good. The front edge accumulation volume is approximately 4.3 million m^3, leading to the damming of the mainstream of the Jinsha River, as shown in Fig. 2(a).

With the large range of the "Xiaguiwa" landslide, part of the slope has not completely evolved into a landslide. According to the rock formations exposed on the surface, the "Xiaguiwa" slope is divided into four areas, A, B, C, and D, as shown in Fig. 2(b). Area A is the main sliding area of the landslide and is currently in a stable state. The rock formations in this area are severely bent and broken, occurring at E90° ∠45°. The middle and upper parts expose the sliding bed controlled by the lithological interface. The middle and lower parts retain a good stepped landslide platform, with an "upper concave and lower convex" bending deformation. Area B is located on the left-wing of Area A and is

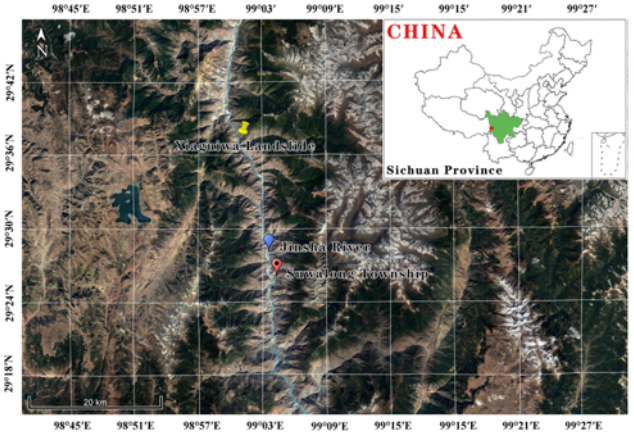

Fig. 1. Location of the "Xiaguiwa" Landslide

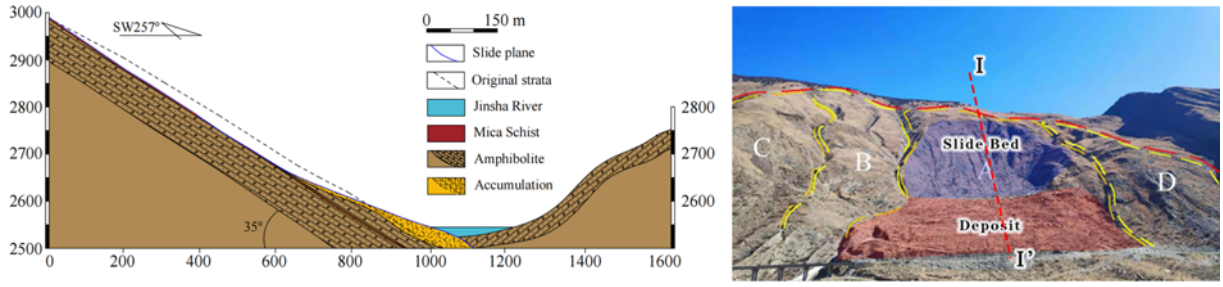

Fig. 2. Overview of Research Slope: (a) Section 'I-I' of the "Xiaguiwa" Landslide, (b) Topography of the "Xiaguiwa" Slope

in a stage of slight rock formation slippage and bending. Many obvious depressions on the slope surface indicate signs of multilevel collapse in this area. Area C is at the stage of bending and uplifting of the bottom rock layer; the degree of rock layer bends sharply as the height decreases (Fig. 3(a)). Area D is located on the right-wing of Area A. The upper rock layer has collapsed, the rear edge shows a cracked depression, and the rock layer is uplifted and fractured at the foot of the slope (Fig. 3(b)). According to the structural characteristics of the "Xiaguiwa" bedding landslide and the failure phenomena appearing in each area, the formation mechanism of the landslide can be summarized as follows: slight rock slip and bending stage, bottom rock bending and uplift stage, uplift surface fracture and fragmentation stage, and low shear out stage.

According to field investigations, we obtained the structural characteristics of the rock layers in the study area were obtained: hornblende layers from the slope surface to 3 m depth, mica schist interlayer from 3 m to 5 m depth, and hornblende layers below 5 m depth; landslide deposits composed of mica schist were exposed in the road excavation near the toe of area A (Fig. 4(a)). As shown in Fig. 4(b), a more obvious buckling failure phenomenon can be seen. The slope of area A is relatively stable, with good weak and hard rock structure and obvious "buckling failure" phenomenon, so the slope of this area is

Fig. 3. Buckling on Landslide: (a) Curved Uplift Phenomenon of C Area, (b) Uplift and Fracture of Rock Layer in D Area

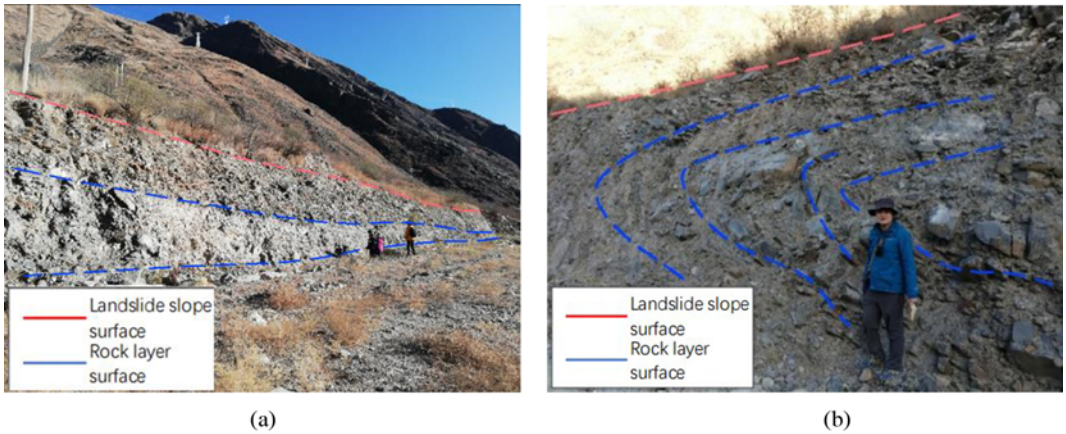

Fig. 4. Rock Layer Interface: (a) Rock Layer Level, (b) Rock Layer with Buckling Failure

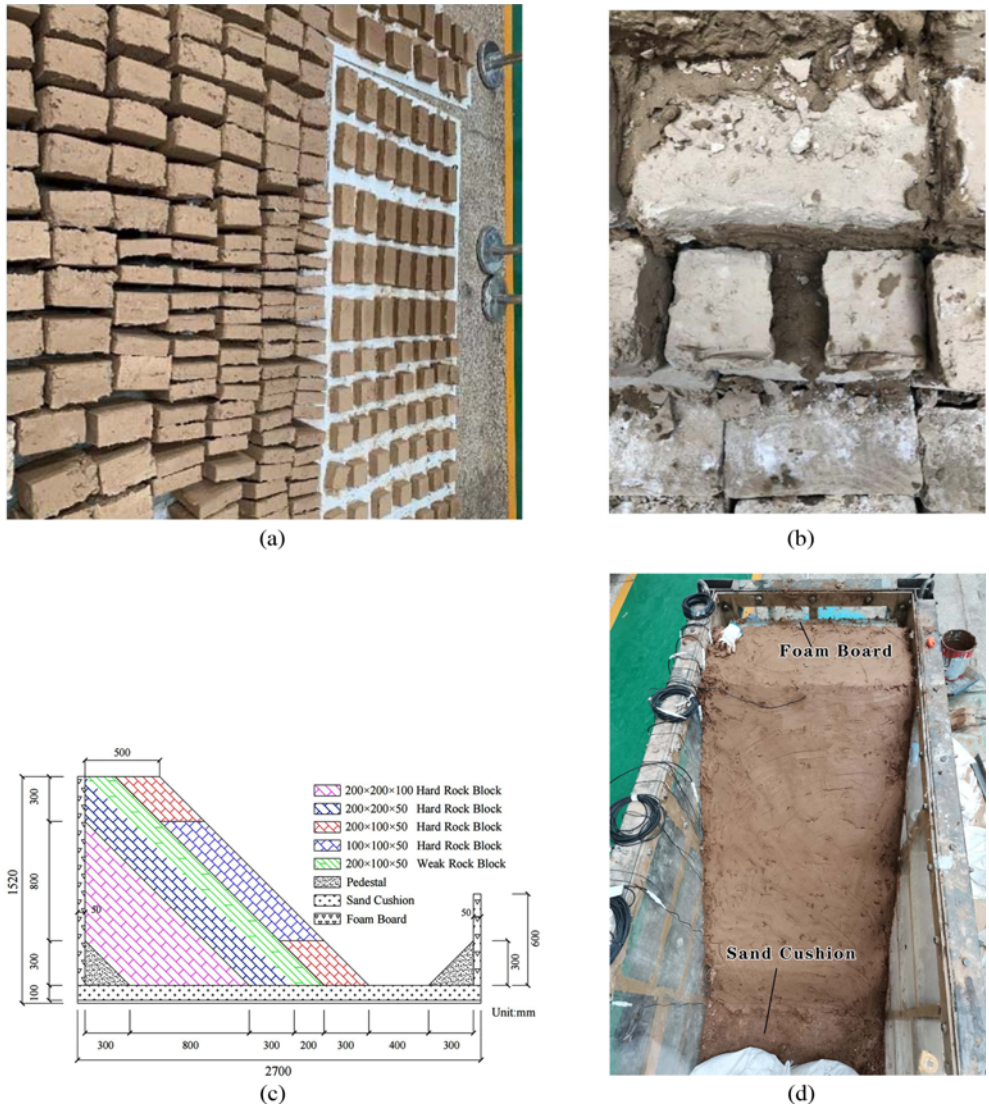

Fig. 5. Design Details of Model Slope: (a) Similar Material Test Block, (b) Diagram of Sensor Positions, (c) Sectional View for Slope Test Model (unit: mm), (d) The Test Model

chosen as the shaking table test prototype.

2.2 Model Slope Size

The test model shown in Fig. 5(c) was designed according to the topographic characteristics, lithology distribution, Structural surface characteristic, shaking table equipment size, and the load of the "Xiaguiwa" landslide. The size similarity ratio of the prototype model is 1:100. The model has a length of 1.9 m, a width of 1 m, and a height of 1.4 m; the rock formation's inclination angle and slope angle are both 45°.

2.3 Similarity Relationship and Material Ratio

A scaled test was used; the prototype and model must satisfy the law of similarity. The experiment was based on the principle of similarity, with length, time, and density as the basic control variables; the similarity relationship shown in Table 1 is derived from the Buckingham π theorem (Buckingham, 1914; Luo and

Table 1. Similarity Ratios of the Model

Parameters	Similarity ratio (C)
Physical dimension (L)	$C_L = 100$
Density (ρ)	$C_\rho = 1$
Time (t)	$C_t = 10$
Frequency (f)	$C_f = 0.1$
Displacement (s)	$C_s = 100$
Acceleration (a)	$C_\alpha = 1$
Elasticity modulus (E)	$C_E = 100$
Cohesive force (c)	$C_c = 100$
Internal fraction angle (φ)	$C_\varphi = 1$
Velocity (v)	$C_v = 10$
Damping ratio (λ)	$C_\lambda = 1$
Stress (σ)	$C_\sigma = 100$
Strain (ε)	$C_\varepsilon = 1$
Poisson's ratio (μ)	$C_\mu = 1$
Gravitational acceleration (g)	$C_g = 1$

Note: L, ρ, and t are the controlling parameters

Table 2. Prototype and Model Parameters

Lithology		Density ρ (kN/m^3)	Cohesive force c (kPa)	Internal Friction angle φ (°)	Dynamic elastic modulus E (GPa)	Poisson's ratio μ
Weak rock	prototype	2.7 – 3.2	3.0 – 5.0	30 – 50	10.0 – 60.0	0.20 – 0.40
	model	3.1	0.038	42	0.1 – 0.6	0.30
Hard rock	prototype	2.7	28.6	47	33.8	0.33
	model	2.5	0.3	44	0.338	0.33

Ge, 2008).

Based on the indoor physical mechanics' test results and the rock mechanics parameters in the Geotechnical Engineering Handbook, a comparison of the prototype and model parameters is presented in Table 2. Weak rock and hard rock test blocks were prepared by changing the ratio of aggregate (barite powder, quartz sand) and cement (silty clay, gypsum, and glycerin). The material ratio closest to the mechanical parameters of the prototype was determined through shear and compression tests on the test block, Hard rock material ratio: Silty Clay: Barite powder: Quartz sand: Plaster: Water: Glycerin = 41.3:22.9:11.4: 8.7:14.9:0.8 Weak rock material ratio: Silty clay: Barite powder: Quartz sand: Plaster: Water: Glycerin = 32.3:30.2:11.4:12.4:12.7:1. To simulate the difference between hornblende and mica schist more realistically, in addition to the different ratios, the sizes of weak and hard rocks are also different, with blocks of 50 mm thickness selected for weak rocks and 100 mm thickness for hard rocks.

2.4 Model Slope Construction

To simulate the thick and thin rock layer characteristics and complex joint distribution of the prototype slope, the model test block dimensions before the test were 200 × 200 × 100 mm^3, 200 × 200 × 50 mm^3, 200 × 100 × 50 mm^3, and 100 × 100 × 50 mm^3 (Fig. 5(a)). Before constructing the model side slope, a 10 cm thick sand mat was placed at the bottom of the box as a damping layer to reduce the boundary effect caused by the model box structure (Wu et al., 2020). A polyethylene closed-cell foam plate with a thickness of 5 cm was placed on each side of the box wall in the vibration direction to reduce the rigid reflection of seismic waves generated at the sidewalls of the model box (Dong et al., 2011; Wu et al., 2020). The model was built from the bottom to the top according to the design shown in Fig. 5(c). The side seams were filled with sand and leveled to ensure an even and flat rock surface, and a mixture of clay-plaster was added between the layers as a binder, while trace amounts of talc were added to make the structural planes more pronounced. To control the inclination of the rock layer, a sand foundation with a height of 30 cm and an inclination angle of 45° was built at the bottom of the slope. The finished model slope is shown in Fig. 5(d).

2.5 Setting Measuring Points

To study the dynamic characteristics and dynamic response laws of the slope under the action of strong earthquakes, acceleration sensors were arranged on the slope surface, lithological interface, and in the slope in the experiment (Fig. 5(b)). Sensor A0 was located on shaking table to record the true acceleration state of the input seismic wave; Sensors A1 – A3 were located in the thick hard rock area in the middle. Sensors A4 – A7 were located at the boundary between the thick hard rock and the thin hard rock to monitor changes in the acceleration response of the thick hard rock and layer thickness differences. Sensors A8 – A12 and A13 – A17 were located in weak upper and lower interfaces of the interlayer to monitor the influence of lithological differences on the acceleration response law. Sensors A18 – A22 were located on the slope surface to monitor the acceleration response law at the slope surface and the slope shoulder. To explore the trend of the slope surface and vertical acceleration changes in the slope, the sensors were arranged on the same horizontal and vertical surfaces. The acceleration sensors arrangement is shown in Fig. 6.

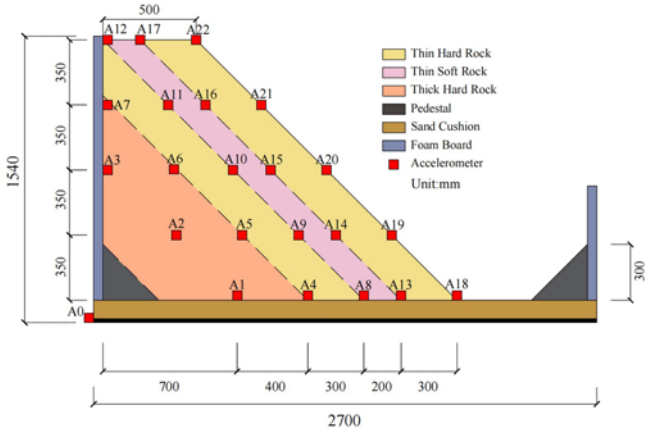

Fig. 6. Schematic Model Layout and Location of Instrumentation

2.6 Loading System

The landslide area is located in the upper reaches of the Jinsha River at the junction of Sichuan and Tibet, with bare surface bedrock and a seismic activity environment similar to Wenchuan, Sichuan. Thus, the measured seismic waves at Maoxian station and Wolong station in the Wenchuan earthquake catalog and sine waves were selected as the inputs. The Maoxian seismic wave lasted 300 s, with a peak acceleration of 0.3 g and a magnitude of 8.0 Ms. The type is bedrock ground motion, the same as that in the Qinghai-Tibet Plateau. The Wolong seismic wave lasted 180 s, with a peak acceleration of 1.0 g and a magnitude of 8.0 Ms. The type is soil layer ground motion. This natural ground motion can accurately simulate the seismic environment of the landslide

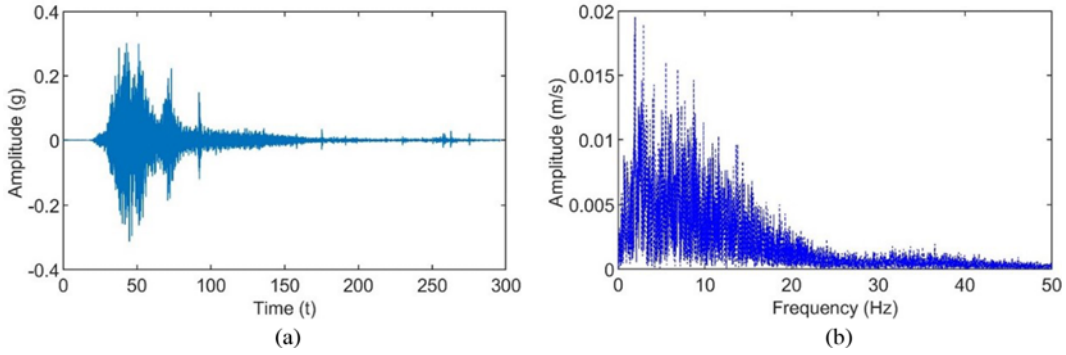

Fig. 7. Maoxian Seismic Wave of Wenchuan Earthquake: (a) The Time History, (b) The Fourier Spectrum

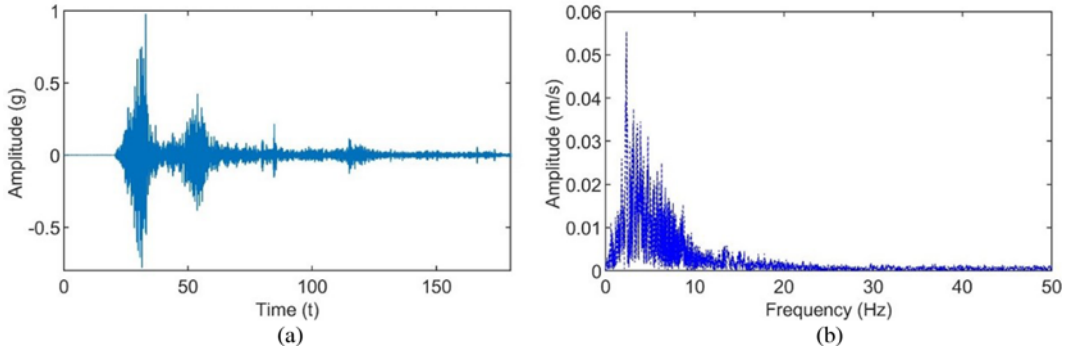

Fig. 8. Wolong Seismic Wave of Wenchuan Earthquake: (a) The Time History, (b) The Fourier Spectrum

Table 3. Test Load Sequences

No.	Stage	Load	Amplitude	Frequency	Duration
1		WN	0.1		60
2 – 4		Sine wave	0.1	5, 10, 15	30
5		WN	0.1		60
6 – 8	I	Sine wave	0.15	5, 10, 15	30
9		WN	0.1		60
10 – 12		Sine wave	0.2	5, 10, 15	30
13		WN	0.1		60
14 – 25	II	MX–WN	0.3 – 0.8		30
26 – 28	III	Sine wave	0.9 – 1.1	10	30

WN is short for White Noise

area and enhance the site-specificity of the dynamic response of the model slope. The horizontal Maoxian seismic wave and Wolong seismic wave of the Wenchuan earthquake are shown in Figs. 7 and 8. Detailed loading conditions are shown in Table 3.

3. Slope Dynamic Response Analysis

3.1 Variation Law of Slope Natural Vibration Characteristics

Acceleration response law of slope can directly reflect the dynamic response law of slope, and the dynamic characteristics can inner reflect the dynamic response law of slope, the slope of the dynamic characteristics can be obtained by applying white noise excitation in the experiment, in the shaking table test research on dynamic characteristics of the slope mainly concentrated in the slope of the change of natural frequency and damping ratio.

The natural frequency of the slope was derived by calculating the transfer function for each measuring point. In the shaking table model test, excited by white noise, the absolute acceleration transfer function of a certain side point is expressed as

$$H_a(\omega, z_i) = \frac{G_{XY}(\omega, z_i)}{G_{XX}(\omega)}. \tag{1}$$

The frequency corresponding to the peak point of the transfer function can be regarded as the natural frequency of each order. After normalizing the peak value of the transfer function for each measurement point, the acceleration mode was obtained. The half-power bandwidth method is used to calculate the damping ratio, expressed as

$$\lambda = \frac{(\omega_2 - \omega_1)}{2\omega_0}. \tag{2}$$

The test results show that under the excitation of white noise, the transfer function has peak points of 28.32 Hz, 37.59 Hz, and 47.36 Hz, which are the first-, second-, and third-order natural frequencies, respectively, as shown in Fig. 9. As the input amplitude increases, the natural frequencies of slopes I, II, and III are reduced. With an increase in the number of vibrations, the I mode is always significant; the II and III modes are gradually coupled and difficult to identify. This indicates that the slope is affected mainly by the first-order natural frequency, and there is

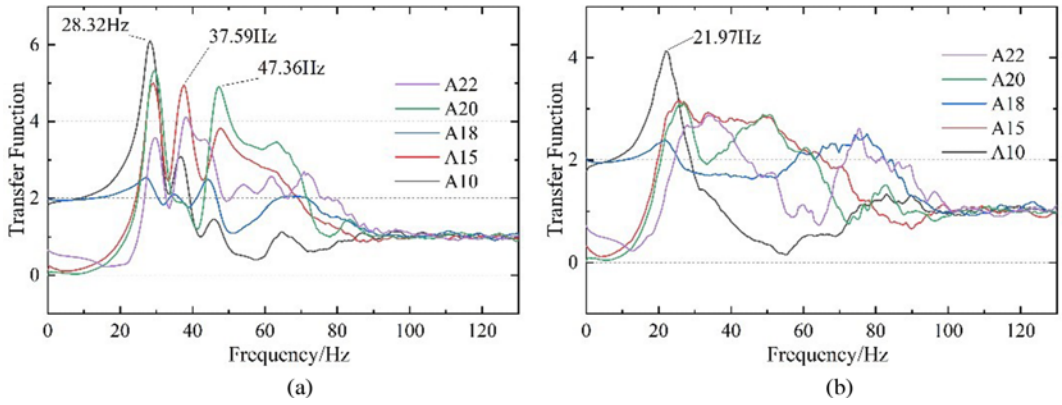

Fig. 9. Transfer Function Characteristics: (a) Measuring Point under Working Condition 1, (b) Measuring Point under Working Condition 23

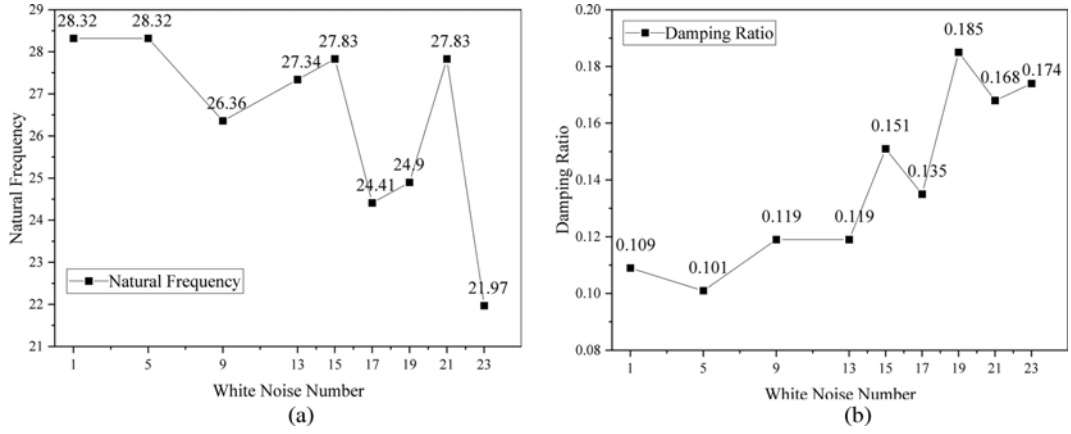

Fig. 10. Changes in Dynamic Characteristic: (a) Changes in Natural Frequency, (b) Changes in Damping Ratio

a tendency to approach the low-frequency first-order mode.

From Figs. 10(a) and 10(b), due to the complexity of slope damage under earthquake action, the curve fluctuates, the overall trend is that the natural frequency of the slope decreases, the damping ratio increases, and the stability of the slope decreases after repeated strong earthquakes. After the natural wave inputs of 0.3 g and 0.6 g (conditions 15, 21) in Maoxian, the natural frequency of the slope decreased rapidly, the shear strength of the slope body decreased, and the overall rigidity decreased, indicating that the overall structure of the slope body underwent significant changes.

3.2 Acceleration Response Law

To study the slope acceleration response law, the PGA (peak ground acceleration) amplification coefficient (the ratio of peak acceleration at slope measurement points to peak acceleration at table measuring points) was used as the seismic response parameter for each measuring point in the slope.

According to the similarity, the natural wave is compressed according to the time similarity ratio of 1:10 to obtain the Wenchuan seismic wave with a duration of 30 s and a dominant frequency of 19.52 Hz. The compressed seismic waves were used for analysis.

Analysis the Maoxian wave the with time compression ratio of 10, the variation law of PGA amplification coefficient with amplitude at different heights under horizontal ground motion is shown in Fig. 11. A3 and A7 are located in front of the shock-absorbing foam board. The displacement space is small, so the PGA amplification coefficient is lower than other positions. The PGA amplification coefficient gradually increases from inside to the surface of slope, reflecting the "surface-tending effect" of dynamic acceleration response. As the input amplitude increases, the PGA amplification coefficient at the bottom of the slope is generally less than 1 because the sand bedding absorbs part of the seismic energy, and the "surface-tending effect" is weakened. It is considered that the rock layer at the bottom of the slope is relatively stable, and no displacement or deformation occurs. When the seismic wave propagates to the slope's surface and passes through the weak rock layer and its upper and lower surfaces, the difference of PGA amplification coefficient indicates the unevenness of the seismic wave being amplified. The acceleration effects at the bottom, 1/4, 3/4, and 1/2 heights, are the same. The PGA amplification coefficients are negatively correlated with the input amplitude, and there are abrupt changes in the PGA amplification coefficients at some locations; when the input seismic wave amplitude increases from 0.6 g to 0.7 g, the PGA coefficients at each location increase abruptly, and the slope is considered to be damaged under the 0.6 g amplitude ground motion combine

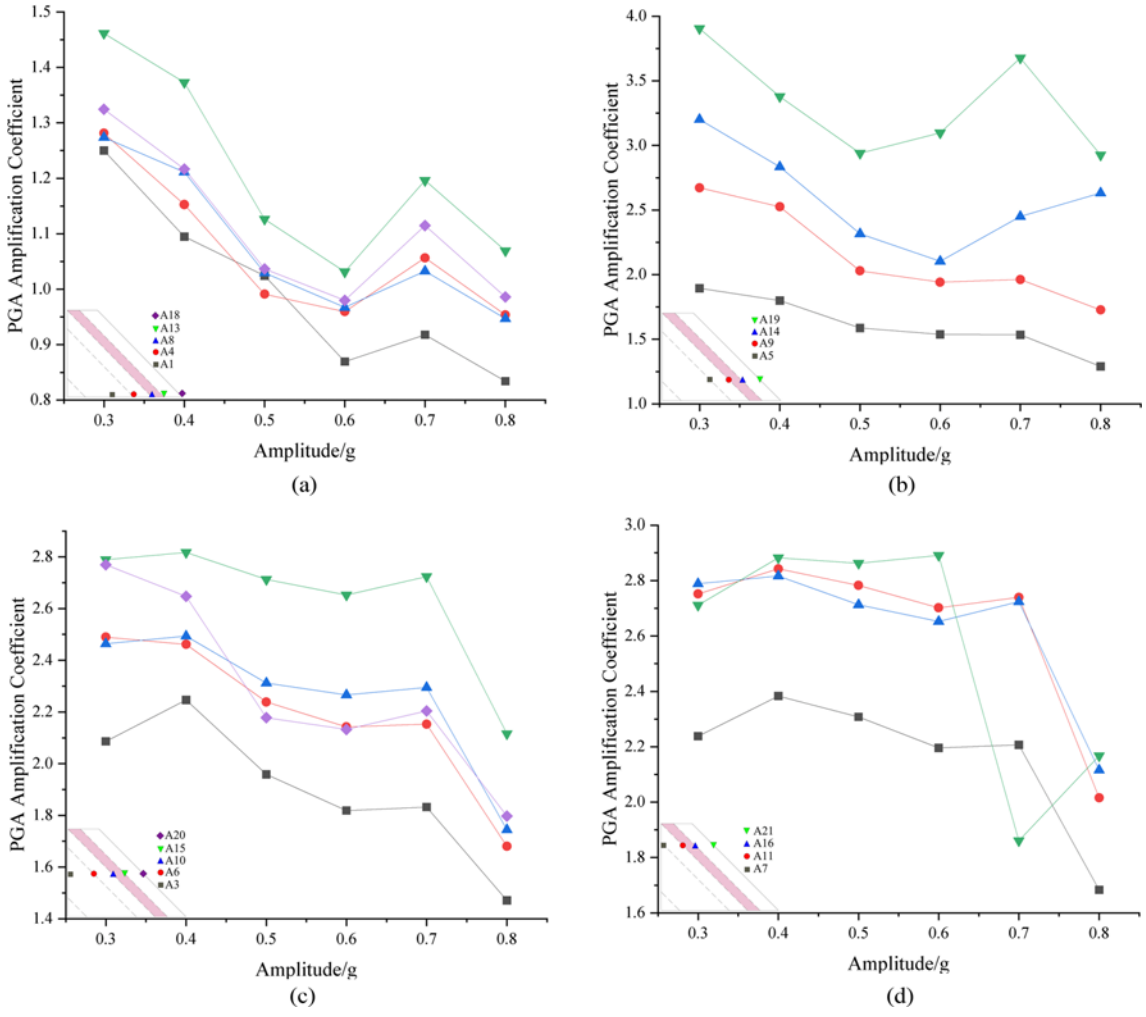

Fig. 11. PGA Amplification Coefficient for Each Measuring Point in the Slope: (a) Bottom of Slope, (b) 1/4 Height of Slope, (c) 1/2 Height of Slope, (d) 3/4 Height of Slope

the analysis in section 3.1. The dynamic response law of the slope has a strong correlation with the ground surface-tending. The law of the PGA amplification coefficient at different horizontal positions in the slope is roughly the same, but the numerical difference is large. The PGA amplification coefficient is the largest at 1/4 height of the slope, where the rock layer is severely deformed, resulting in uneven bending of the whole bedding rock layer.

4. Influence of Weak Rock Interlayer

In the process of seismic wave propagation in the model slope, the weak rock layer is often the first place where earthquake damage occurs, so it is very important to study the displacement and acceleration response on both sides of the weak rock layer.

4.1 Influence of Weak Rock Interlayer on Acceleration Response

To analyze the influence of the weak rock layer on the slope under the action of seismic waves, the contours of the peak acceleration of the slope and the PGA amplification coefficient curves of A5, A9, A14, A19 and A6, A10, A15, A20 at different amplitudes are plotted.

As shown in Figs. 12 and 13, the peak acceleration is greatest at 1/4 height of the slope under Maoxian wave. The peak acceleration increases significantly at the weak rock layer, which indicates that the weak interlayer plays an amplifying role on the seismic wave, but there is a weak reduction of the seismic wave at the weak rock layer at the buckling height of the slope. Overall the weak rock layer plays an enhancing role on the seismic waves, which leads to more instability near the weak rock layer. Our result are contrary to that obtained by Chen et al. (2016) and Du et al. (2021), which may be related to the type of weak rock layer.

4.2 Influence of Weak Rock Interlayer on Acceleration Response Spectrum

Maoxian natural waves (0.4 g, 0.6 g, and 0.8 g) were selected for spectrum analysis. Sensors A8–A13 and A10–A15 were selected on the upper and lower interfaces of the weak rock layer as the position reference. The fast Fourier transform (FFT) was performed

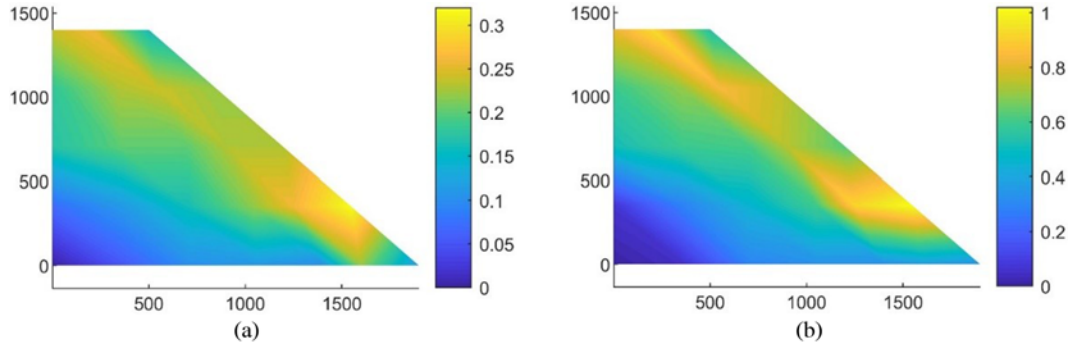

Fig. 12. The Contour of Peak Acceleration: (a) 0.2 g Maoxian Wave, (b) 0.6 g Maoxian Wave

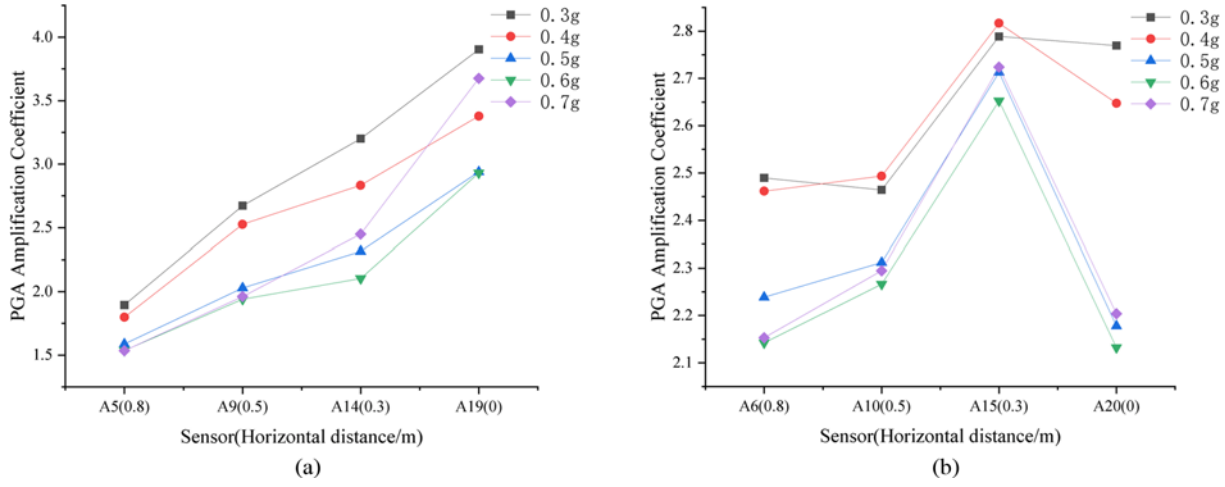

Fig. 13. The Acceleration at Different Heights is Affected by Weak Rock Layer: (a) 1/4 Height, (b) 1/2 Height

on the acceleration time history curve for each sensor to obtain the corresponding velocity frequency domain curve.

As is shown in Fig. 14. Comparing the data from two sets of measurement points with the same input amplitude, it is found that the frequency spectrum of the seismic wave near the weak rock layer can be divided into two frequency bands: 0 – 30 Hz and 30 – 60 Hz, with a limit of 30 Hz. The frequency at the bottom of the slope is concentrated from 0 – 30 Hz; the frequency ranges from 15 – 40 Hz. The seismic stress propagates in the solid framework and the pores and cracks, producing material friction, consuming vibration energy, and causing the natural frequency to shift downward (Xu et al., 2010). The bottom and middle interlayer affect the seismic wave spectrum, producing a different transformation effect. The bottom interlayer amplifies the seismic wave from 30 – 60 Hz, and the middle interlayer reduces the seismic wave from 30 – 60 Hz. As the amplitude of the input seismic wave increases, the weak rock interlayer more significantly amplifies and attenuates the seismic wave from 30 – 60 Hz. This test verifies the influence of weak rock interlayers on seismic dynamic response; at different heights, the upper and lower interfaces of the weak rock may enlarge or reduce the high-frequency range of seismic waves. This differential modification effect causes the seismic waves to be uneven. In the upper hard rock layer, concave and convex bending deformation of the whole rock layer is produced, demonstrating the influence of the weak rock interlayer on the seismic dynamic response of the slope.

5. Analysis of Slope Failure Characteristics

5.1 Analysis of Maximum Displacement of Measuring Point in the Slope

Six sensors on the weak and hard lithology interface and three on the slope table were selected as the research samples. The acceleration time history curve represents quadratic integration and zero line callback; the maximum displacement in the time domain is used to analyze the slope in working conditions 0.6 g – 0.8 g Maoxian wave. The calculation results are shown in Figs. 15 and 16.

As the amplitude of the natural wave input increased, the maximum displacement of each point in the slope gradually increased; the maximum displacement in the slope always occurred at the upper interface in the middle of the weak rock interlayer. The upper interface of the weak rock layer develops upward and downward; the overall displacement of the upper interface in the middle of the weak rock interlayer is larger than that of the other two layers. It is speculated that this layer is the control surface of the slope sliding; the overall displacement in the lower half of the slope is greater than in the upper half of the slope, proving that bending and fracture of the lower rock layer require more displacement space. The displacement cloud map in Fig. 17 is drawn according to the

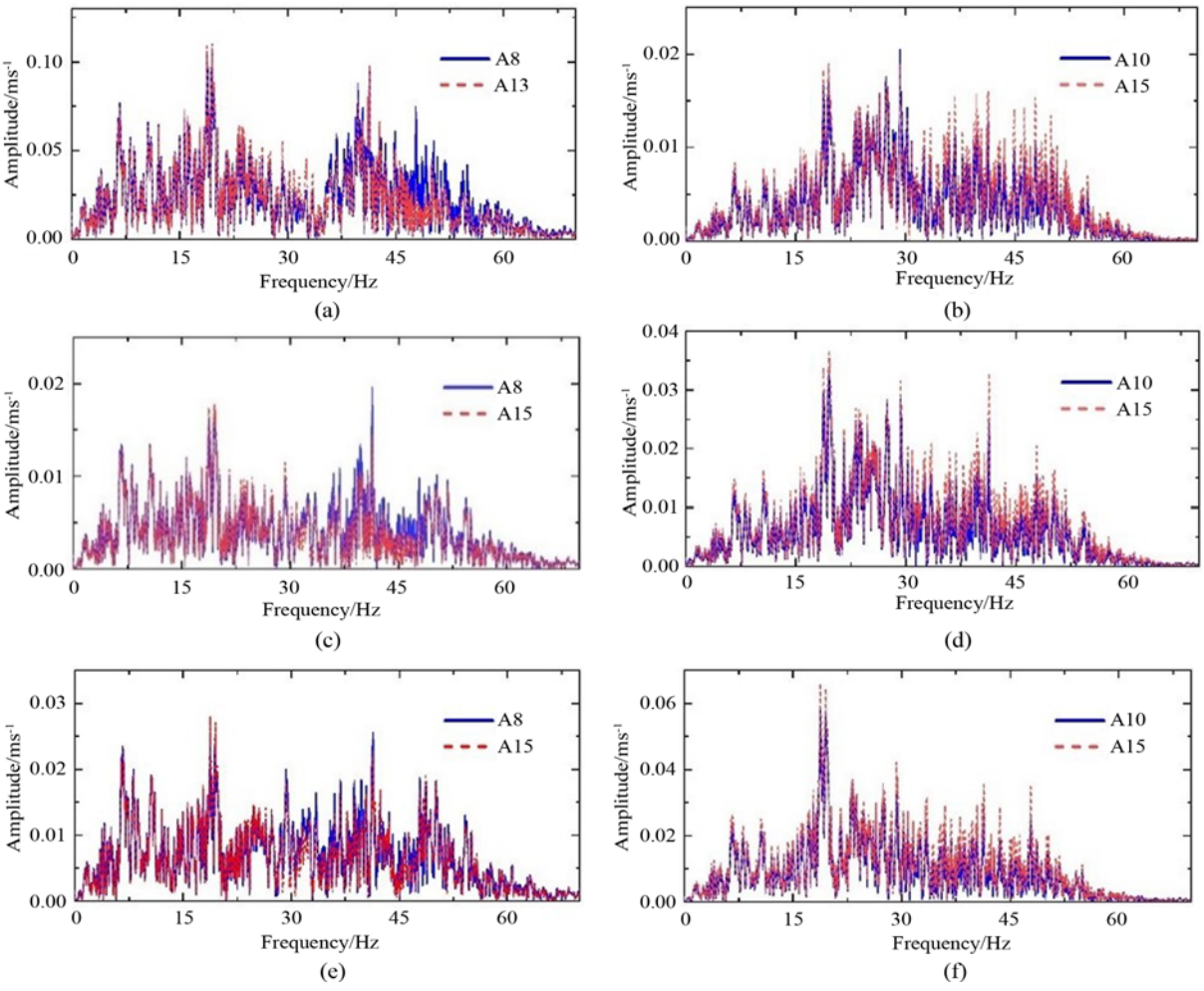

Fig. 14. Fourier Spectrum Characteristics: (a) A8 and A13 at 0.4 g, (b) A10 and A15 at 0.4 g, (c) A8 and A13 at 0.6 g, (d) A10 and A15 at 0.4 g, (e) A8 and A13 at 0.8 g, (f) A10 and A15 at 0.8 g

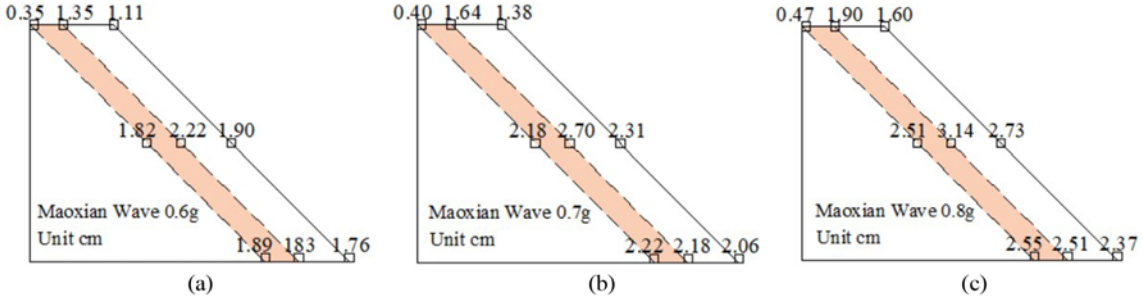

Fig. 15. Displacement in Slope with Different Amplitude Inputs (direction: right): (a) 0.6 g Maoxian Wave, (b) 0.7 g Maoxian Wave, (c) 0.8 g Maoxian Wave

displacement distribution law of the slope; the "upper concave and lower convex" deformation law is obtained, which is consistent with the experimental phenomenon and the original "Xiaguiwa" landslide. The structural features are consistent.

5.2 Slope Model Instability Mode and Deformation and Failure Characteristics

The instability deformation and failure of the model slope were the most intuitive results obtained in the test. A high-speed camera arranged before the test recorded the entire process of deformation and failure of the slope subjected to strong earthquakes.

After the input of low-frequency sine wave (5-15 hz, 0.1-0.2 g), the layer line is about 1 cm lower than the initial layer line, as shown in Fig. 18(a), and the drop is most significant in the weak rock layer, while the rock layer is slightly bent. When the input amplitude of Maoxian natural wave reaches 0.6 g, the slope starts to show signs of fragmentation, as shown in Fig. 18(b), and the uplift first occurs at the quarter height of the slope, and the bending

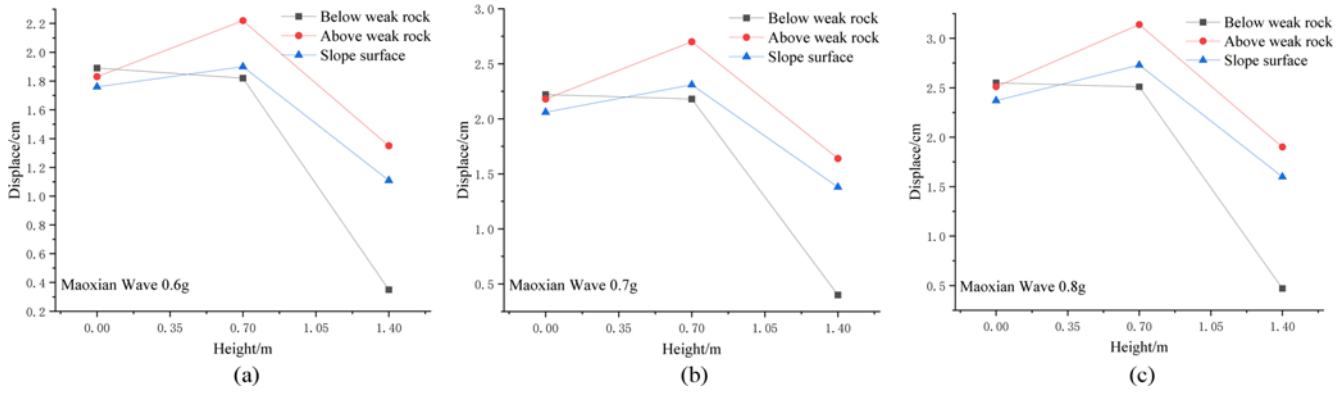

Fig. 16. Displacement Curves in Slope with Different Amplitude Inputs: (a) 0.6 g Maoxian Wave, (b) 0.7 g Maoxian Wave, (c) 0.8 g Maoxian Wave

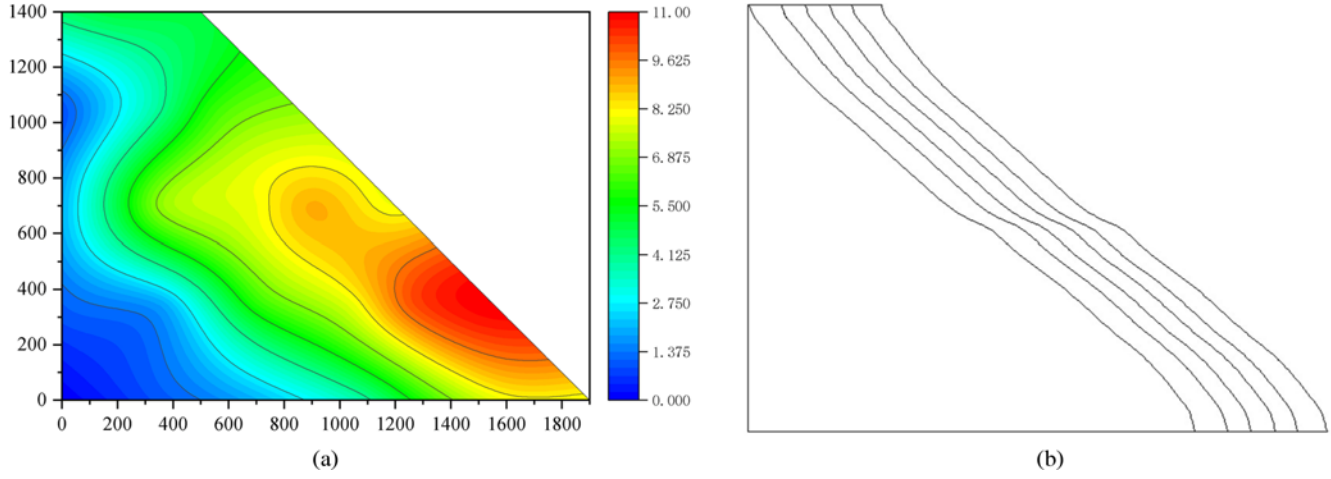

Fig. 17. Conceptual Diagram of Rock Formation Deformation: (a) Displacement Vector Diagram, (b) Slope Deformation Diagram

of the rock layer increases. When the Maoxian natural wave input amplitude reaches 0.8 g, the slope deformation becomes more serious. The upper rock layer sinks, the rock bending of the slope increases, the thin rock layer at the slope toe shows obvious signs of upward bending; the weak rock layer at the waist of the slope has a small amount of depression, and the weak rock layer slides slightly downward. The thick hard rock layer at the bottom of the slope is destroyed, and the width of cracks increases. As shown in Figs. 18(c) and 18(d), the rock layer below the top of the slope sinks and bends obviously. When 10 Hz 1.1 g sine wave is input, the whole slope is destabilized and the rock layer slips and fractures as a whole. The "bulge" and bending can be seen from the side, as shown in Figs. 18(e) and 18(f). The slope shoulder is severely broken, with obvious tension fractures. The sliding of the thin rock layer is greater than that of the thick rock layer; the thin rock layer bends at the intersection of the thin and thick rock layers. The rock layer below half of the slope is more broken than the rock layer above half; "buckling" occurs at the height of the slope in the outermost quarter of the rock layer.

According to the macro-experiment phenomenon, the instability deformation failure process of the model slope can be divided into four stages: slight rock settlement and bending stage, bottom rock layer bending and uplift stage, uplift surface fracture and fragmentation stage, and low shear out stage. The rock thickness and the weak and hard lithology interface are the controlling joint surfaces for slope sliding. The rock sliding surface, the slope toe shear slip surface, and the upper tensile fracture surface are connected to form a complete slip surface.

6. Conclusions

Based on the analysis of slope response, deformation, and failure, the following conclusions were obtained:

1. With the increase of vibration times, the natural frequency of the slope decreases, the damping ratio increases, and the internal stability of the slope decreases. By observing the change of natural frequency and PGA amplification coefficient of slope, it can be inferred that 0.3 g and 0.6 g are the critical dynamic conditions of the slope cracking and instability. With the increase of the amplitude of the input wave, the PGA amplification coefficient decreases at all parts of the slope. The PGA amplification coefficient at 1/4 height is greater than that at other heights, resulting in serious deformation here.
2. Overall schist-like weak rock layers amplify seismic waves, but at 'bucking' heights, weak rock layers attenuate seismic waves. At the slope toe, the weak rock layer amplifies the

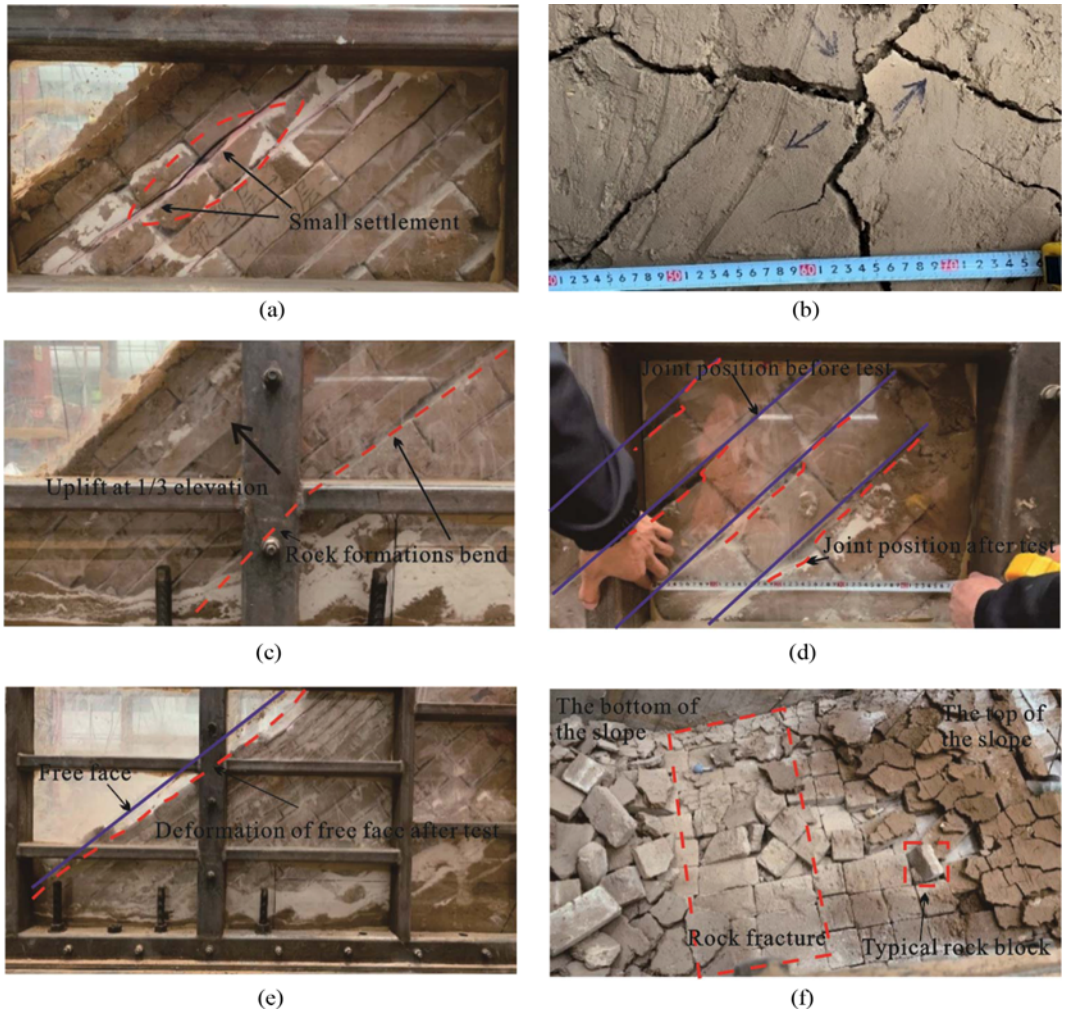

Fig. 18. Failure Process of Slope Model: (a) Small Settlement of Rock Layer, (b) Uplift at the 1/4 Height, (c) Rock Layer Bend at the Slope Toe, (d) Thick Rock Fracture, (e) Fallen Thin Hard Rock Layer, (f) Overall Condition of Slope Surface Fragmentation

low-frequency waves and filters the high-frequency waves, and with the increase of the height, the amplification of the high-frequency band increases again gradually, and at the middle of the slope, it presents a uniform amplification of the seismic waves. Maximum displacement often occurs above weak rock layer. Uneven amplification and reduction of seismic waves in weak rock layer causes rock layer to bend and deform, forming "concave" and "convex" shapes.

3. As the input amplitude increases, the whole slope appears to settle and slip between the layers, and the degree of deformation increases. "Break" occurs at one-fourth of the height of the slope surface, and the rock layer in the slope has "upward concave and downward convex" deformation characteristics. According to the experiment phenomenon, the instability deformation failure process of the model slope can be divided into four stages: the slight bending and settlement stage of the rock layer, the bending and uplift stage of the bottom rock layer, the breaking and fragmentation stage of the uplift surface, and the low shearing stage.

Shaking table tests were used to study the dynamic response law and deformation and failure characteristics of bedding rock slopes with schist-like weak rock layer, revealing the starting position of slope deformation and failure, controlling joints and failure processes, treating bedding rock landslides in the Jinsha River basin, and providing a basis for mitigating engineering disasters.

Acknowledgements

The research was financially supported by National Key R&D Program of China (Grant No. 2018YFC1505001).

ORCID

Chen Wang https://orcid.org/0000-0003-2476-9626
Kunsheng Gu https://orcid.org/0000-0001-6632-7135

References

Abe K, Nakamura S, Nakamura H, Shiomi K (2017) Numerical study on dynamic behavior of slope models including weak layers from

deformation to failure using material point method. *Soils Found* 57(2):155-175, DOI: 10.1016/j.sandf.2017.03.001

Aydan Ö (2016) Large rock slope failures induced by recent earthquakes. *Rock Mechanics and Rock Engineering* 49(6):2503-2524, DOI: 10.1007/s00603-016-0975-3

Buckingham E (1914) On physically similar systems, illustrations of the use of dimenional equations. *Physical Review Journals Archive* 4(4):345-376, DOI: 10.1103/PhysRev.4.345

Chen ZL, Hu X, Bu XB (2020) Effect of weak intercalation on failure mode of rock slopes under seismic excitation. *Natural Hazards* 105(1):363-381, DOI: 10.1007/S11069-020-04314-Z

Chen ZL, Hu X, Xu Q (2016) Experimental study of motion characteristics of rock slopes with weak intercalation under seismic excitation. *Journal of Mountain Science* 13(3):546-556, DOI: 10.1007/s11629-014-3212-0

Chigira M, Wang WN, Furuya T, Kamai T (2003) Geological causes and geomorphological precursors of the Tsaoling landslide triggered by the 1999 Chi-Chi earthquake, Taiwan. *Engineering Geology* 68(3-4):259-273, DOI: 10.1016/S0013-7952(02)00232-6

Clough RW, Pirtz D (1956) Earthquake resistance of rock-fill dams. *Journal of the Soil Mechanics and Foundations* 82(2):1-26, DOI: 10.1061/JSFEAQ.0000010

Deng TX, Ju NP, Li LQ, Jiang YB, Zhang CY (2016) Study on dynamic unstability mehanism of alopes with interbredded soft and hard rock beddings. *Science Technology and Engineering* 16(36):133-138

Deng ZY, Liu XR, Liu YQ, Liu SL, Han YF, Liu JH, Tu YL (2020) Model test and numerical simulation on the dynamic stability of the bedding rock slope under frequent microseisms. *Earthquake Engineering and Engineering Vibration* 19(4):919-935, DOI: 10.1007/s11803-020-0604-8

Dong JY, Yang GX, Wu FQ, Qi SW (2011) The large-scale shaking table test study of dynamic response and failure mode of bedding rock slope under earthquake. *Rock and Soil Mechanics* 32(10):2977-2988, DOI: 10.16285/j.rsm.2011.10.012

Du RF, Fei XJ, Jia J, Zhang XC, Yang S (2021) Experimental study on rock slope with weak interlayer under blasting seismic wave. *China Civil Engineering Journal* 54(4):95-106, DOI: 10.15951/j.tmgcxb.2021.04.010

Fan G (2016) The dynamic response and time-frequency method for seismic stability evaluation of layered rock slope with weak intercalated layer. PhD Thesis, Southwest Jiaotong University, Chengdu, China (in Chinese)

Fan G, Zhang JJ, Fu X, Zhou LR (2016a) Dynamic failure mode and energy-based identification method for a counter-bedding rock slope with weak intercalated layers. *Journal of Mountain Science* 13(12):2111-2123, DOI: 10.1007/s11629-015-3662-z

Fan G, Zhang JJ, Wu JB, Yan KM (2016b) Dynamic response and dynamic failure mode of a weak intercalated rock slope using a shaking table. *Rock Mechanics and Rock Engineering* 49(8):3243-3256, DOI: 10.1007/s00603-016-0971-7

Hoek E, Bray JD (1981) Rock slope engineering. CRC Press, London, UK

Huang RQ, Li G, Ju NP (2013) Shaking table test on strong earthquake response of stratified rock slopes. *Chinese Journal of Rock Mechanics and Engineering* 32(5):865-875

Huang RQ, Pei XJ, Li TB (2008) Basic characteristics and formation mechanism of the largest scale landslide at Daguangbao occurred during the Wenchuan earthquake. *Journal of Engineering Geology* 16(6):730-741

Jia J (2011) Study on dynamic responses and failure mechanism of steep bedding rock slope triggered by strong earthquake. MSc Thesis, Chengdu University of Technology, Chengdu, China (in Chinese)

Li YY, Feng XY, Yao AJ, Lin S, Wang R, Guo MZ (2021) A massive ancient river-damming landslide triggered by buckling failure in the upper Jinsha River, SE Tibetan Plateau. *Bulletin of Engineering Geology and the Environment* 80(7):5391-5403, DOI: 10.1007/s10064-021-02293-4

Li LQ, Ju NP, Zhang S, Deng XX, Sheng DC (2019) Seismic wave propagation characteristic and its effects on the failure of steep jointed anti-dip rock slope. *Landslides* 16(1):105-123, DOI: 10.1007/s10346-018-1071-4

Liu CZ (2014) Genetic types of landslide and debris flow disasters in China. *Geological Review* 60(4):858-868

Liu HX, Xu Q, Zou W, Xu HB (2012) Shaking table test for vertical dynamic resonse behavior of layered rock slopes. *Journal of Vibration and Shock* 31(22):13-19, DOI: 10.13465/j.cnki.jvs.2012.22.003

Luo XQ, Ge XR (2008) Theory and application of model test on landslide. China WaterPower Press, Beijing, China, 7-33

Lv Q, Liu YR, Yang Q (2017) Stability analysis of earthquakeinduced rock slope based on back analysis of shear strength parameters of rock mass. *Engineering Geology* 228(10):39-49, DOI: 10.1016/j.enggeo.2017.07.007

Men YM, Peng JB, Li XC, Hao JB (2004) Research on vibration testing of models for dynamic stability of rock slope with layered structures. *World Earthquake Engineering* 20(4):131-136

Song DQ, Che AL, Zhu RJ, Ge XR (2019) Natural frequency characteristics of rock masses containing a complex geological structure and their effects on the dynamic stability of slopes. *Rock Mechanics and Rock Engineering* 52(11):4457-4473, DOI: 10.1007/s00603-019-01885-7

Wang SH, Cun JF (2008) Study on failure mechanism and stability of the bedding rock slope. *West-China Exploration Engineering* 2008(10):13-16

Wartman J, Seed RB, Bray JD (2005) Shaking table modeling of seismically induced deformations in slopes. *Journal of Geotechnical and Geoenvironmental Engineering* 131(5):610-622

Wu DH, Liu YQ, Li HB, Xia X, Peng B, Shen H (2020) Shaking table tests on dynamic amplification and failure mechanism of layered rock slopes under seismic actions. *Chinese Journal of Rock Mechanics and Engineering* 39(10):1945-1956, DOI: 10.13722/j.cnki.jrme.2020.0033

Xu Q, Dong XJ (2011) Genetic types of large-scale landslides induced by Wenchuan earthquake. *Earth Science* 36(6):1134-1142

Xu Q, Liu HX, Zou W, Fan XM, Chen JJ (2010) Large-scale shaking table test study of acceleration dynamic responses characteristics of slopes. *Chinese Journal of Rock Mechanics and Engineering* 29(12): 2420-2428

Xu GX, Yao LK, Gao ZN, Li ZH (2008) Large-scale shaking table model test study on dynamic characteristics and dynamic responses of slope. *Chinese Journal of Rock Mechanics and Engineering* 27(3):624-632

Yang GX, Wu FQ, Dong JY, Qi SW (2012) Study of dynamic response chatacters and failure mechanism of rock slope under earthquake. *Chinese Journal of Rock Mechanics and Engineering* 31(4):696-702

Zhang D, Wu ZJ, Liang QG, Zhao DG, Liang C, Li FX (2019) Shaking table test study of displacement and acceleration response characteristics of loess slope surface. *China Civil Engineering Journal* 52(S2):162-169, DOI: 10.15951/j.tmgcxb.2019.s2.023

Zhou YF, Liu HX, Zhu X, Wen JH (2020) Modal analysis of rock slope with a weak interlayer and its influence on seismic dynamic response of slope. *Earthquake Engineering and Engineering Dynamics* 40(1):223-232, DOI: 10.13197/j.eeev.2020.01.223.zhouyf.022

Zhou F, Xu Q, Liu HX, Wang L (2016) An experimental study of dynamic response characteristics of slope with horizontal weak interlayer under earthquake. *Rock and Soil Mechanics* 37(1):133-139, DOI: 10.16285/j.rsm.2016.01.016